IL NUOVO CIMENTO Vol. 30 C, N. 5 Settembre-Ottobre 2007
DOI 10.1393/ncc/i2008-10261-1

Photodetector and scintillation crystals requirements for gamma-ray imaging(*)

R. Pani(1), M. N. Cinti(2), R. Pellegrini(1), P. Bennati(2), S. Lo Meo(3), S. Ridolfi(2), F. Vittorini(2), F. de Notaristefani(4) and M. Mattioli(2)

(1) *INFN-Roma I and Dipartimento di Medicina Sperimentale, Università "La Sapienza" Rome, Italy*
(2) *INFN-Roma I and Dipartimento di Fisica, Università "La Sapienza" - Rome, Italy*
(3) *INFN-Bologna and Dipartimento di Fisica dell'Università - Bologna, Italy*
(4) *INFN-Roma III and Dipartimento di Ingegneria Elettronica, Università di Roma III Rome, Italy*

(ricevuto il 3 Marzo 2008; pubblicato online il 24 Aprile 2008)

Summary. — The diffusion of the PET and SPET techniques in different applications, like investigation on small organs and tissues or animal imaging, has induced in the past years the researchers to develop modular scintillation cameras to have compactness and versatility in order to obtain dimensions and configurations suitable to the particular application. To this purpose different photodetectors have been studied, as an alternative to the photomultiplier tubes (PMT) based on semiconductor technology. At the same time new scintillating crystals have been tested to match the requirements like high light yield or fast decay time, needed for SPET and PET application, respectively. In this paper we have investigated the photodetector and scintillation crystals requirements to optimize a gamma-ray imager based on scintillation crystals. To this aim we show results about the principal parameters characterizing a gamma-ray imaging, like energy and spatial resolution. The performances of a continuous $LaBr_3$:Ce crystal ($49 \times 49 \times 4\,mm^3 + 3\,mm$ glass window) are compared to the ones from a pixellated and continuous NaI:Tl crystal, coupled to multi-anode photomultiplier tube (Hamamatsu H8500 MA-PMT). Furthermore the results are supported with Monte Carlo simulations. With the lanthanum detector, we obtain 1.1 mm of intrinsic spatial resolution, comparable with that predicted by the MC simulations. We test also the new ultra bialkali PMT Hamamatsu R7600-200 with a QE = 42%, obtaining an improvement in terms of energy resolution of about 25%, respect to a standard PMT, with a $LaBr_3$:Ce cylinder ($1/2''\phi \times 1/2''$ thickness).

PACS 21.60.Ka – Monte Carlo models.
PACS 87.61.Ff – Instrumentation.
PACS 87.63.-d – Non-ionizing radiation equipment and techniques.

(*) Paper presented at the 1st Workshop on Photon Detection for High Energy Medical and Space Applications; Perugia, June 13-14, 2007.

1. – Introduction

The diffusion of molecular imaging in different applications, like investigation on small organs and tissues or animal imaging, has induced in the past years the researchers to develop modular scintillation cameras to have suitable dimensions and configurations for PET and SPET techniques.

Different photodetectors, based on semiconductor technology like silicon P-I-N detectors, avalanche photodetectors (APDs), silicon drift detectors (SDDs) and silicon photomultiplier (SiPM), have been studied, as an alternative to the photomultiplier tubes (PMT), to improve new dedicated detectors.

In this paper we have investigated, with the support of literature and experimental data, the photodetector and scintillation crystals requirements to optimize a gamma-ray imager. To this purpose we introduce the two principal techniques of positioning for these detectors, that is light sharing and individual coupling, and present a short review of the state of art of the scintillator crystals. Subsequently, we show results about the principal parameters characterizing a gamma-ray imaging, like energy and spatial resolution, obtained with the last generation of scintillator crystals, like $LaBr_3$:Ce crystal, and multi-anode photomultiplier (MA-PMT). The results are supported with Monte Carlo simulations.

Moreover, since the new generation of photodetectors like SiPM presents a high degree of quantum efficiency (QE $\sim$ 70%) we extend the analysis also to the effective improvement due to the high QE in scintillation detectors based on light sharing techniques. To this aim, we study the response in terms of energy resolution of a new photomultiplier with ultra bialkali window (UBA) recently developed by Hamamatsu coupled to a $LaBr_3$:Ce scintillation crystal. We focus the attention on the influence of the geometric configuration of the detector and the high QE of the photodetector on the imager spatial resolution, utilizing MC simulations.

2. – Light output readout: individual coupling and light sharing

The two principal light output readouts are the individual coupling and the light sharing. The difference between these two techniques is substantially on the position calculation method. The individual coupling technique is based on the direct coupling of an individual scintillation crystal with a single photodetector to obtain a single detecting element with an individual electronic readout. This technique is essentially used in PET application and each element represents a position coordinate in the overall gamma-ray imager. Therefore it is necessary to provide each element with an individual electronic readout.

In fig. 1, as an example, a single module of the PET-scanner MADPET II detector [1] dedicated to small animal imaging, utilizing the individual coupling technique, is shown. MADPET-II consists of 18 dual-layer detector modules arranged in a 71 mm diameter ring. Each module consists of a 4×8 array of $2\,\text{mm} \times 2\,\text{mm} \times 6\,\text{mm}$ LSO crystals, each optically isolated and coupled one-to-one to a monolithic APD array (Hamamatsu Photonics, Japan). The individual crystals are separated by a 0.3 mm layer of high-reflectance multilayer polymer mirror foil to match the pitch of the APD array and to optimize light collection.

In the light sharing technique the light distribution coming from a scintillation event is sampled by an array of photodetectors, like the PMTs array in Anger Camera or anodes in MA-PMT. For this technique the position of the event is calculated applying the centroid algorithm on the signals coming from each photodetector. So it is possible to

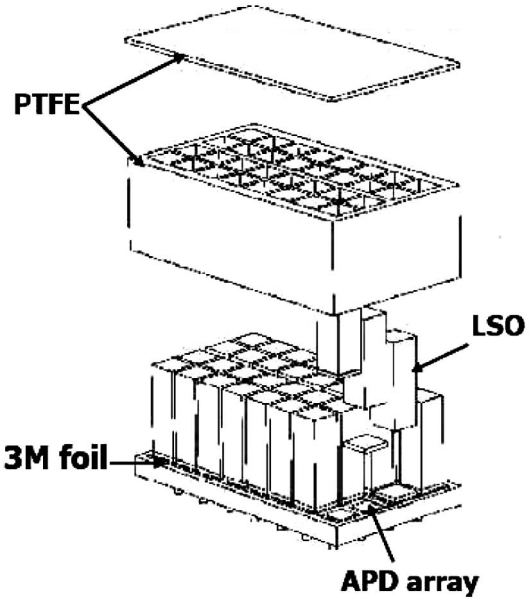

Fig. 1. – Single module of MADPET II.

utilize single-element readout, like in PET, or resistive chain readout, that represents a cheaper solution, especially in large FoV detector (like Anger Camera). In fig. 2 the light sharing technique is summarized: on the left the point spread function of a continuous crystal is shown, while on the right the result of the scintillation light sampling by an 8×8 anodic array of a MA-PMT, in terms of collected charge, is reported.

The position of the event is calculated by the formula

$$X_c = \frac{\sum_j n_j x_j}{\sum_j n_j}, \tag{1}$$

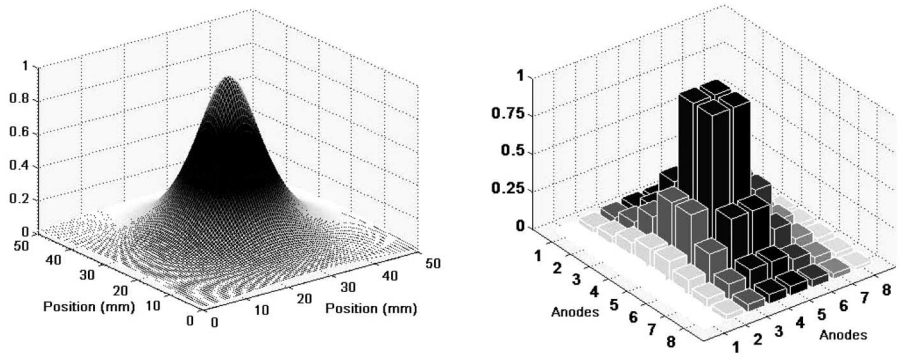

Fig. 2. – Light sharing technique. On the left the light distribution coming from a single scintillation event, for a continuous scintillation crystal. On the right the sampling from the 8×8 anodes array of the H8500 MA-PMT (single-channel readout).

TABLE I. – *Individual coupling ad light sharing technique characteristics.*

	Individual coupling	Light sharing
Packing fraction	High	High
Energy resolution	Poor uniformity—depending on scintillator/photodetector	High—depending on scintillator/photodetector design
Spatial resolution	Limited by pixel crystal size	Excellent for continuous crystal (depending on crystal thickness)
Electronic readout	Large number of chains (up to 20000)	Low number of chains
Light collection	Poor	Good
Single photoelectron readout	Not needed	Needed
Gain	Not high ($\sim 10^4$)	High (about 10^6)
Cost	Expensive	Inexpensive

where $n_j = \sum_k n_j^k$ is the "projection" of the charge collected along the j-th column, x_j is the anode coordinate along the x direction and X_c is the centroid coordinate along the x direction. The same applies along the Y direction. In any case it is possible to realize array detectors in order to optimize the imager dimensions to specific applications.

In table I, the comparison between these techniques, in terms of detector characteristics, is reported. While in light sharing pixellated and continuous crystals are utilized, for individual coupling technique only pixellated scintillation crystals can be used. This introduces a limitation in spatial resolution that depends on the pixel size: in fact, for NaI:Tl pixellated crystals the smallest pixel dimension available at the moment is 1 mm, while for the new generation of scintillation crystals, like $LaBr_3$:Ce, the manufacturing of pixellated samples has not been implemented yet. In any case, the pixellated crystals present very good position linearity and also good spatial resolution (better than 1 mm) even utilizing scintillation crystals with a not excellent light yield, like for example YAP. On the contrary the energy resolution is reduced due to the non-homogeneity response of the single pixel ($\sim 15\%$ for 1 mm pixel size NaI:Tl scintillation crystal [2]).

The continuous scintillation crystals show high values of energy resolution, due to homogeneity response and good light collection, and excellent results in terms of intrinsic spatial resolution, especially when scintillators with high light yield are employed. In fact, Pani *et al.* [3] have demonstrated that the standard deviation of point spread function of image can be presented by the formula

$$\sigma_{\mathrm{im}} \propto \frac{\sigma_{\mathrm{lightPSF}}}{\sqrt{n_{\mathrm{phe}}}}\,, \tag{2}$$

where the numerator is the standard deviation of scintillation light spread and the denominator is the square root of the number of photoelectrons produced in the scintillation events. For example, for the new generation of scintillation crystals like $LaBr_3$:Ce with a light yield of 63000 ph/MeV, we have obtained, in integral assembly configuration

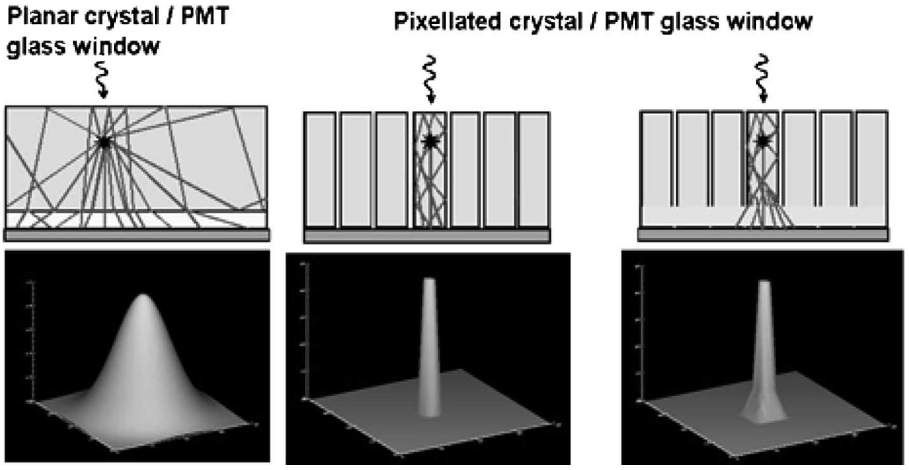

Fig. 3. – Point spread function of the light. On the left the distribution coming from a continuous crystal and on the center and the right the same one from two different configurations of pixellated crystals.

and 5 mm crystal thickness, an intrinsic spatial resolution of 0.9 mm [4]. The Spatial Resolution (SR), linked with the position linearity response (l) by the relation [5]

$$\mathrm{SR} = 2.35 \cdot \frac{\sigma_{\mathrm{im}}}{l} \tag{3}$$

depends also on the machining of the crystal edges and on the crystal thickness [4].

The light collection is another critical aspect of the continuous crystals. The collection efficiency depends on the optimization of the coupling between the scintillation crystal and the photodetector, and is limited by the critical angle.

In particular the maximum collection efficiency, when a scintillation crystal is coupled to a photocathode window, can be calculated by means of the following formula:

$$\mathrm{CE}_{\mathrm{max}} = 1 - \cos\vartheta_c, \tag{4}$$

where θ_c is the critical angle given by

$$\vartheta_c = \sin^{-1}\frac{n_{\mathrm{window}}}{n_{\mathrm{crystal}}}, \tag{5}$$

where n_{window} and n_{crystal} are the refractive indices of the window material and of the scintillation crystal, respectively. The $LaBr_3$:Ce critical angle is about 52°. If the angle of incidence of the light incoming on the crystal-window interface is greater than this value, a total reflection will occur with a consequent reduction of the light collected on the photocathode. In fig. 3 the light distributions coming from continuous and pixellated crystals are shown. The internal reflection inside the continuous crystal and the thickness induce a larger point spread function of the light respect to the pixellated one, where the incidence angle results less than 45°. Although a reduction in light emission is observed, the pixellated structure is better than the continuous one in the optimization of the light collection efficiency of the detector.

TABLE II. – *Requirements in SPET/PET.*

	SPECT	PET
Z	≥ 40	≥ 50
Density	High > 3 g/cc	High > 7 g/cc
Decay time	$< 1\,\mu$s	< 300 ns
Luminosity efficiency	High > 20000 ph/MeV	High > 8000 ph/MeV
Afterglow	Low	Low

3. – Scintillation crystal

In table II we summarize the requirements for a scintillation crystal in SPET and PET applications. Both techniques need a high photofraction value, to optimize the energy windowing. A high density of the scintillator is necessary in SPET to obtain 80–90% efficiency also with a reduction of the crystal thickness (for the light collection and packing detection assembly). In PET a high efficiency implies the use of a small length crystal (30 mm) to avoid 50% coincidence efficiency and to reduce parallax error, as used in small animal imaging application. A short decay time is a very important requirement in PET in order to allow good coincidence time resolution; in particular time resolution better than 0.5 ns can reduce random coincidences (50% in a 3D PET) and time of flight can be realized. Otherwise in SPET high luminosity efficiency is determining to improve decoding crystal pixel in the scintillation array, energy resolution and spatial resolution in continuous crystals. This feature is in any case useful also in PET to enable block detectors with a greater number of pixels and to reduce scatter background (25% Compton scattering/25% "true" events in a 3D PET), improving energy resolution. For both techniques a low afterglow of the crystal is important to obtain a high counting rate.

In table III the characteristics of the principal scintillators utilized today in SPET and PET are reported. Analyzing these values we can individuate in the new generation of *cerium*-doped scintillators, like $LaCl_3$:Ce, LuI_3:Ce and mainly $LaBr_3$:Ce the best materials to be utilized in both SPET and PET techniques, respectively. In table the energy resolution ($\Delta E/E$) is reported at energy photon values where the scintillators are principally utilized (140 and 511 keV for SPET and PET, respectively).

4. – Equipment

4˙1. *Energy and spatial resolution measurements.* – In this work we utilized two continuous crystals, a $LaBr_3$:Ce and NaI:Tl scintillator with the same identity ($49 \times 49 \times 4\,\text{mm}^3 + 3$ mm glass window), a cylindrical $LaBr_3$:Ce ($1/2''\phi \times 1/2''$ thick) crystal and a pixellated NaI:Tl with $1 \times 1 \times 4\,\text{mm}^3$ pixel size. The continuous crystals walls are treated to optimize the response in imaging application (white back and black edges), while the cylindrical crystal has the walls white painted to optimize the light collection for spectroscopic measurements.

The $LaBr_3$:Ce scintillator (BrilLiance$^{\text{TM380}}$ - Saint Gobain [6]) represents a new generation of scintillation crystals. It shows very interesting properties for the gamma-ray

TABLE III. – *Characteristics of scintillation crystal. Courtesy of Van Ejk C. W. E.*

	Density (g/cm^3)	Z eff	Photo-fraction (%)	Light yield (ph/MeV)	Decay time (ns)	$\Delta E/E$ (PMT)	Emiss. max (nm)
BGO	7.1	83	43 (511 keV)	9000	300	10% (511 keV)	480
YAP	5.50	36.0	50 (140 keV)	21000	27	20% (140 keV)	350
Lu_2SiO_5:Ce (LSO)	7.4	65	34 (511 keV)	26000	40	10% (511 keV)	420
$Lu_{2(1-x)}Y_{2x}SiO_5$:Ce (LYSO)	7.1	54	-	30000	40	11% (511 keV)	420
$LaCl_3$:Ce	3.86	49.5	80 (140 keV) 15 (511 keV)	40000	27 (65%)	8% (140 keV) 4% (511 keV)	350
NaI:Tl	3.67	51.0	84 (140 keV)	41000	230	9% (140 keV)	410
$LaBr_3$:Ce	5.07	47.4	79 (140 keV) 14 (511 keV)	70000	16 (97%)	6% (140 keV) 3% (511 keV)	380
CsI:Tl	4.51	52.0	86 (140 keV)	66000	630	14% (140 keV)	565
LuI_3:Ce	5.60	-	90 (140 keV) 29 (511 keV)	90000	30	<15% (511 keV)	472 535

imaging application: a very high light output at a wavelength suited for the bialkali photocathode (63000 light photons/MeV at 380 nm) and a very small non-proportionality with impinging photon energy (less than 5%). These characteristics permit to obtain very good energy resolution (2.9% and 6.6% FWHM at 662 keV and 122 keV photon energy, respectively). In addition, the crystal has very good radiation absorption properties, high photofraction comparable to NaI:Tl, and high speed (16 ns of scintillation decay time), interesting for PET application. The material is hygroscopic.

For the evaluation of energy resolution we utilized a standard photomultiplier Hamamatsu R6231. This PMT presents a QE of 30%, a gain factor of 2.7×10^5 at 1000 V and only 8 stages of multiplication. In particular the voltage divider was modified by Saint Gobain to better match the signal from the lanthanum crystal that presents a high light yield and a fast decay time. The electronic readout was a standard electronic chain for spectroscopic measurements.

We tested also the new ultra bialkali (UBA) Hamamatsu R7600-200 PMT, with QE = 41.6%, to evaluate the improvement in terms of energy resolution utilizing a high QE. This PMT has 10 stages of multiplication and a gain $= 2 \times 10^6 + 06$ at 700 V. In fig. 4 the plot of the quantum efficiency and photocathode radiant sensitivity as a function of wavelength is reported [7].

The continuous and the pixellated NaI:Tl crystals were utilized also for spatial resolution measurements. In this case we coupled the scintillation crystals with a MA-PMT Hamamatsu H8500, which is based on metal channel dynode technology and presents very compact size: the external dimensions are $52 \times 52 \times 14.4\,mm^3$ for an active area of $49 \times 49\,mm^2$, and 1.5 mm glass window. The anodic structure consists of an 8×8 matrix in which each individual anode has a 6 mm side, with an anode gain variation of a factor of 2. The flat panel PSPMT was connected to an independent 64 channel anode

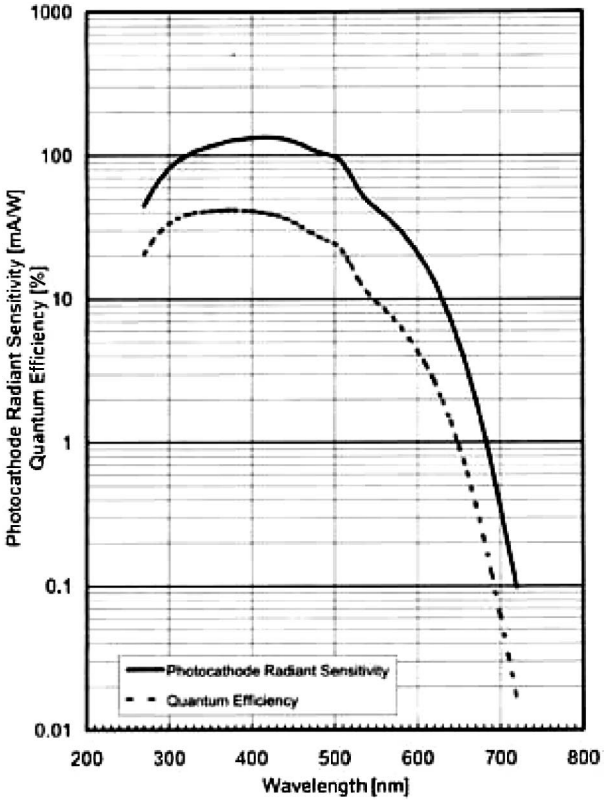

Fig. 4. – Quantum efficiency and photocathode radiant sensitivity as a function of wavelength of Hamamatsu R7600-200.

electronic readout, developed by Southampton University [8]. The system readout is completed by a National Instruments DAQ 6110E card to sample and digitize the anode signals and to address it for the storing to a PC.

To quantify the spatial resolution and the position linearity response, a scanning of the scintillation crystal with a Tc^{99m} (140 keV) 0.4 mm point source was made, at 1.5 mm step.

4˙2. *Monte Carlo simulation.* – The Monte Carlo simulation was developed in GEANT4 code [9, 10]. Geant4 Monte Carlo is an object oriented toolkit for simulation of current (and next generation) HEP detectors. It is also a showcase example of technology transfer from particle physics to other fields such as medical science. It is possible to make accurate modeling of radiation sources, detectors devices and human bodies with easy configuration and friendly interface and at the same time with great precision of physics. The simulation regarded principally the $LaBr_3$:Ce crystal. The crystal is surrounding by a thin layer of aluminium. In the crystal front, after aluminium, there is a very small layer of teflon. The scintillation photons were generated as a pure Poisson process and the intrinsic resolution of the crystal was not considered. The simulated crystal was wrapped in a material acting as a Lambertian reflector (teflon on front) or black absorber (aluminium). The boundary processes followed the rules of the glisur

model (ex GEANT3). As in the experimental set-up, the simulated crystal was coupled to the PMT with a glass layer, 4.5 mm thick including the glass window of the scintillator (3 mm) and PMT (1.5 mm). The PMT surface was built as a polished quartz window, assuming an experimentally derived value for quantum efficiency. The optical properties of the materials involved in the simulations refraction index, absorption and scattering lengths were gathered from various sources. The GEANT4 application was run to record the scintillation light distribution on the MA-PMT anodic plane in order to quantify both spatial and energy resolution.

5. – Results and discussions

5˙1. *Energy resolution.* – The Energy Resolution (ER) of a gamma imager based on a scintillation crystal depends on various components, related to the intrinsic properties of the scintillator, the statistics underneath the physical process of detection, and the characteristics of both the photodetector and processing electronics. The dependence of the energy resolution on these components can be analytically described with the following formula [9]:

$$\mathrm{ER}(E_\gamma) = \frac{\Delta E_\gamma}{E_\gamma} = 2.355 \cdot \sqrt{(R_{\mathrm{e.sci}})^2 + \left(\frac{\alpha}{\eta \cdot N_{\mathrm{ph}}}\right)^2 + \left(\frac{ENC}{\eta \cdot N_{\mathrm{ph}} \cdot M}\right)^2}, \tag{6}$$

where the first term is the scintillator intrinsic contribute depending on the non-homogeneity of the material, in terms of light yield, and non-proportionality of scintillation response to the energy deposited in the crystal. The second term is typically the statistical noise where N_{ph} is the number of photons produced in a scintillation flash, α accounts for the worsening of the Poisson behavior and η is the quantum efficiency. The last term is the electronic noise depending on the photodetector and readout system, where ENC is the Equivalent Noise Charge [11] and M is the multiplication gain.

In table IV we summarize some results found in the literature for different scintillation crystals coupled to standard light detectors. The best value is obtained with $LaBr_3$:Ce crystal coupled with a standard PMT such as a SDD.

In table V, our results for lanthanum continuous crystal in terms of energy resolution as a function of photon energy, with standard photomultiplier Hamamatsu R6231 are reported. The value at 122 keV is compared with the same ones obtained with continuous and pixellated NaI:Tl. The energy resolution value for the pixellated crystal is worsening respect to the continuous one due to the non-homogeneity response of the pixels. In table we show also the results obtained with two samples of lanthanum crystal, manufactured in 2005 and 2004, respectively. We report the manufacturing year to highlight that the improvement in terms of energy resolution could be related to the better quality of the crystal.

The experimental results are in agreement with the expected ones. In fact, fixed to 4.6% and 6.6% the intrinsic energy resolution for $LaBr_3$:Ce and NaI:Tl crystal respectively, and utilizing in formula (1) the parameters for R6231 PMT, we obtained theoretical values of 7.1% and 9.55% for lanthanum and sodium iodine scintillator, respectively.

5˙2. *The new ultra bialkali PMT (UBA).* – Recently Hamamatsu has equipped a one-inch PMT with a new ultra bialkali (UBA) photocathode that permits to obtain QE values greater than 40%. Since the energy resolution depends on the number of photoelectron produced on photocathode, we tested the improvement in energy resolution due

TABLE IV. – *Energy resolution for different scintillation cameras.*

Crystal	Overall ER(%) at 662 keV	ER(intrin.) (%)	ER(stat.) (%)	ER(noise) (%)	Light detector
NaI:Tl	6.7	5.9	3.2	0	PMT[(a)]
CsI:Tl	6.6	5.8	3.2	0	PMT XP2254B Philips [12]
CsI:Tl	4.3	3.8	1.5	1.2	SDD [13]
$LaBr_3$:Ce	3.6	2.2	2.5	0	PMT XP20Y0 Photonis [14]
$LaBr_3$:Ce	2.7	2.0	1.7	0.5	SDD [15]
LSO	8.8	7.8	3.6	0	PMT XP20Y0 Photonis [14]
BGO	11.7	5.8	8.0	0	PMT XP20Y0 Photonis [14]
YAP	4.3	2.5	2.3	2.6	APD–6307073500 Adv.Phot.Inc [16]

[(a)] Standard.

to this new photocathode coupling the $LaBr_3$:Ce cylinder ($1/2''\phi \times 1/2''$ thickness) with an R7600-200 PMT with a QE = 42%. In fig. 5 we report the results in comparison with the same ones obtained with a R6231 PMT and H8500 MA-PMT. The values are similar to the data from R6231, so considering the different high-voltage values fixed for these PMTs (−700 V and −1000 V for R7600-200 and R6231, respectively), an improvement is expected in energy resolution and as a consequence in spatial resolution when this technology will be applied on position sensitive PMT. To have a visual evaluation of the

TABLE V. – *Energy resolution result vs. photon energy.*

Energy (keV)	Hamamatsu R6231 + continuous LaBr ($49 \times 49 \times 4\,mm^3$) (2006)	Hamamatsu R6231 + LaBr cylinder ($2''\phi \times 2''$ thick) [17] (2005)	Photonis XP20Y0QDA + LaBr ($10 \times 10 \times 5\,mm^3$) [14] (2004)
60	9.8%	10.6%	13.0%
81	8.6%	9.3%	10.0%
122	6.8% [9.5% continuous NaI:Tl] [14% pixellated NaI:Tl]	6.9%	8.0%
356	4.0%	4.3%	-
511	3.3%	3.1%	4.0%

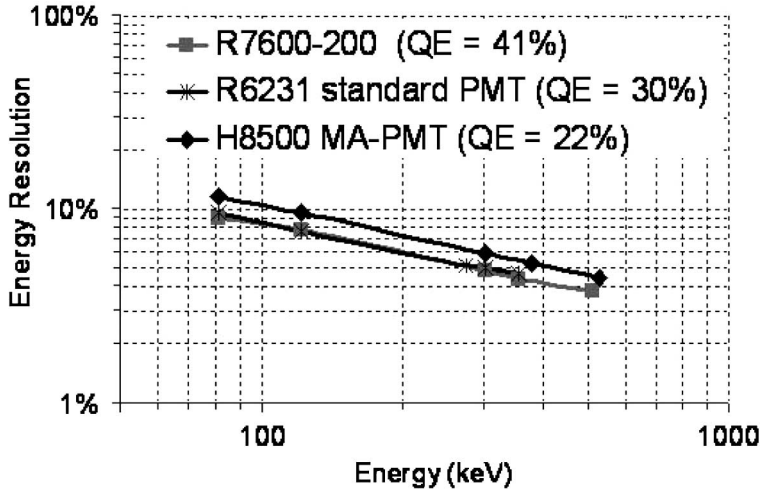

Fig. 5. – Energy resolution *vs.* photon energy for R7600-200 PMT.

performances of this tube with a $LaBr_3$:Ce crystal, in fig. 6 we report the pulse height distribution of a Ba133 gamma-ray source in comparison with the same one from NaI:Tl continuous crystal coupled to R6231. The features at 274 and 302 keV are well separated as well as the features at 356 and 380 keV photon energy.

5˙3. *Spatial resolution*. – The $LaBr_3$:Ce represents the new frontier of the scintillation crystal for SPET and PET. We evaluated the spatial resolution of the gamma camera based on the continuous lanthanum crystal coupled to H8500 MA-PMT in comparison with the result from MC simulations.

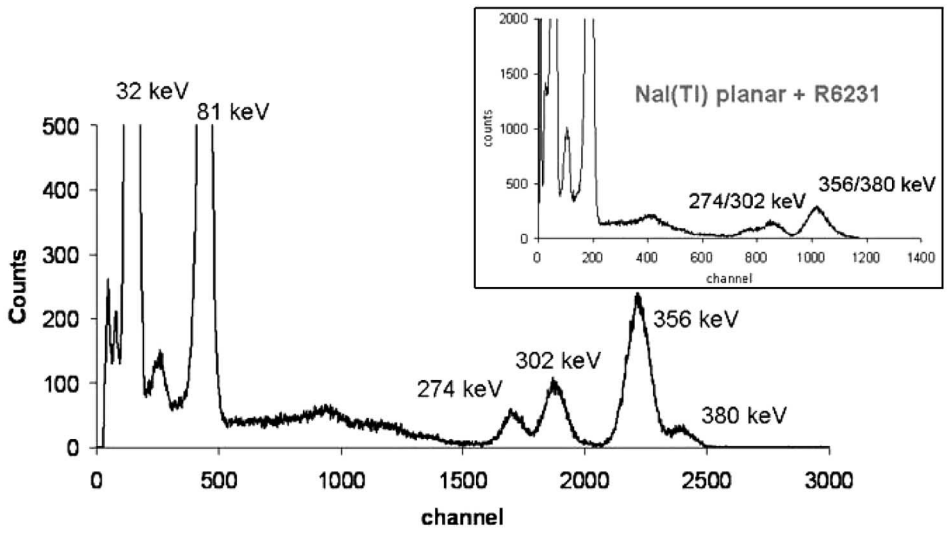

Fig. 6. – Pulse height distribution of Ba133 gamma-ray source from R7600-200 PMT coupled to $1/2'' \times 1/2''$ $LaBr_3$:Ce in comparison with continuous NaI:Tl coupled to R6231 PMT.

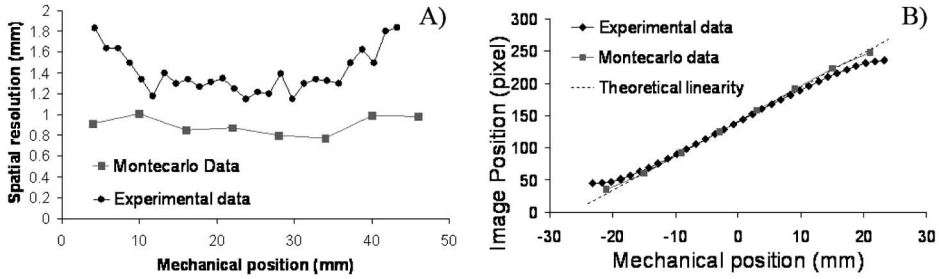

Fig. 7. – Experimental and simulated results for lanthanum camera. A) Spatial resolution and B) position linearity response.

In fig. 7 the results in terms of overall spatial resolution and position linearity are reported. The experimental behavior for spatial resolution is slightly worse respect to the MC simulation, probably due to the contribution of the PMT whereas there is a good agreement in terms of position linearity response. The step scanning simulated with the MC code was 6 mm. The best experimental value of the spatial resolution was 1.1 mm.

5˙4. *Is a high QE really useful?* – We utilized the MC simulation to quantify the expected improvement in terms of spatial and energy resolution when a MA-PMT like the Hamamatsu H8500 will be equipped with a high QE photocathode.

We simulated two values of QE that represent the standard value available at the moment for MA-PMT (22%, for Hamamatsu H8500) and a value (60%) comparable with the new generation of photodetectors like Silicon Photomultiplier (SiPM) or MA-PMT with UBA window. Moreover we selected two different configurations of the scintillation crystal: with 3 mm glass window and without glass window. This last option corresponds to an integral assembly configuration where the scintillation crystal is directly coupled to the photocathode to reduce the glass window thickness and as a consequence to reduce the spread of light distribution collected by the photocathode itself. The lack of glass window reduces the width of the point spread function of the light increasing the light collection. In fig. 8 the simulated charge distributions on an 8×8 anodic plane for three different situations are reported. On the left the standard situation: QE = 22% and crystal glass window. On the right the integral assembly configuration: QE = 22% without crystal glass window. In the center the proposed configuration: QE = 60% without glass window. On the plots are reported also the number of photoelectrons collected on the anodic plane and the energy and spatial resolution values, included the overall value.

Respect to the standard situation we obtained an increase of 61% in the number of photoelectrons collected on anodic plane and a reduction of 9% and 55% of the spatial and energy resolution respectively, only removing the glass window of the scintillation crystal.

A further improvement of the detector response was obtained with high QE values and in particular, a reduction of 20% and 40% of the spatial and energy resolution respectively was observed. This is an interesting result because remarks the importance of utilizing photodetectors with high QE but at the same time focuses on the importance of the geometric effects of the light collection.

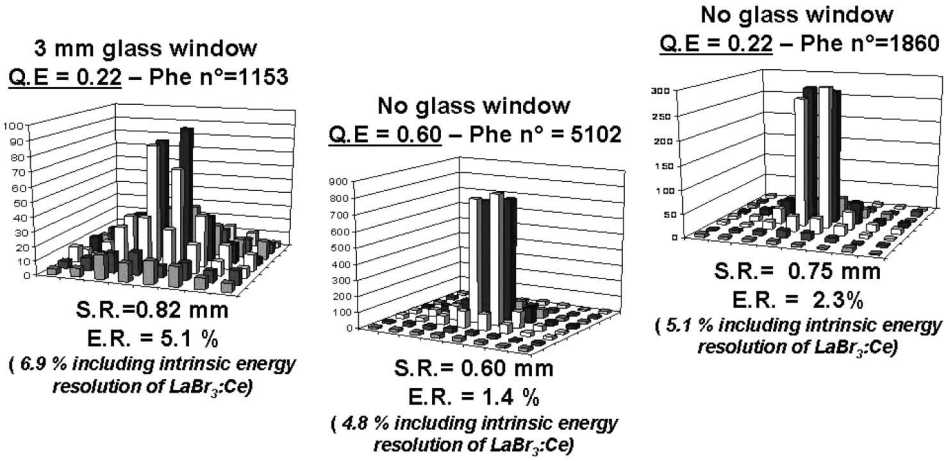

Fig. 8. – MC simulations results about the influence on spatial and energy resolution of the photocathode QE and crystal thickness.

In any case when the intrinsic energy resolution of the crystal is included in the overall energy resolution, the increasing is limited at 30% between the two extreme situations. These values represent a superior limit in the overall energy resolution obtainable with this detector, highlighting the importance of the intrinsic energy resolution of the scintillator in the response of the system.

6. – Conclusions

To optimize a good detector for SPET and PET technique based on scintillation crystal, we have to separate the contribution due to the scintillator and to the photodetector.

The new generation of Ce-doped scintillators, like $LaCl_3$:Ce, LuI_3:Ce and $LaBr_3$:Ce seems to respond to the principal requirements for both techniques, in terms of high light yield, fast decay time and high density. Moreover, the intrinsic energy resolution of scintillators can seriously limit the energy resolution response of photodetectors, so $LaBr_3$:Ce, presenting a low value of this parameter (2% and 4% at 511 and 122 keV, respectively), seems a very promising crystal for SPET and also for time of flight in PET.

About the photodetector, for light sharing configuration with continuous crystal, we need position sensitive photodetectors with superior performances like high quantum efficiency, low electronic noise and good packing fraction. To strongly enhance imaging performances particular crystal/photodetector coupling, like the integral assembly, are also suitable.

The new ultrahigh quantum efficiency PMT opens a new way to get the best imaging performance however the intrinsic energy resolution of scintillators represents a limit in energy resolution response for high QE photodetectors.

REFERENCES

[1] Mcelroy D. P., Pimpl W., Djelassi M., Pichler B. J., Rafecas M., Schuler T. and Ziegler S. I., *First results from MADPET-II: a novel detector and readout system for high resolution small animal PET*, *Nuclear Science Symposium Conference Record, 2003 IEEE, 19-25 Oct. 2003*, Vol. **3**, pp. 2043-2047.

[2] Pani R., Bennati P., Cinti M. N., Pellegrini R., Betti M., Ridolfi S., Lanconelli N., Karimian A., Garibaldi F., Cusanno F., Scafè R., Iurlaro G., Montani L., Marini M., Majewsky S. and de Notaristefani F., *Imaging characteristics comparison of compact pixellated detectors for Scintimammography*, *Nuclear Science Symposium Conference Record, 2004 IEEE, 16-22 Oct. 2004*, Vol. **6**, pp. 3748-3751.
[3] Pani R., Pellegrini R., Cinti M. N., Bennati P., Betti M., Vittorini F., Mattioli M., Trotta G., Orsolini Cencelli V., Scafè R., Navarria F., Bollini D., Baldazzi G., Moschini G. and de Notaristefani F., *Nucl. Instrum. Methods Phys. Res. A*, **571** (2007) 187.
[4] Pani R., Cinti M. N., Pellegrini R., Bennati P., Betti M., Vittorini F., Mattioli M., Trotta G., Orsolini Cencelli V., Scafè R. *et al.*, *Nucl. Instrum. Methods Phys. Res. A*, **576** (2007) 15.
[5] Rogers J. G. *et al.*, *Phys. Med. Biol.*, **31** (1986) 1061.
[6] Scintillation Products Technical Note, "Performance summary: Brilliance TM scintillator $LaCl_3$:Ce and $LaBr_3$:Ce", May 2007.
[7] Hamamatsu Photonics, Technical Sheet R7600-200 (2007).
[8] RUTHERFORD, HX2/RAL/SS System Readout, Applet on Labs Microelectron Group, Tech. Data Sheet, Chilton-Didcot, Oxfordshire UK (1995).
[9] Agostinelli A., Allison J., Amako K. *et al.*, *Nucl. Instrum. Methods Phys. Res. A*, **506** (2003) 250.
[10] Allison J., Amako K., Apostolakis J. *et al.*, *IEEE Trans. Nucl. Sci.*, **53** (2006) 270.
[11] Gatti E., Sampietro M. and Manfredi P. F., *Nucl. Instrum. Methods Phys. Res. A*, **287** (1990) 513.
[12] Allier C. P., Valk H., Huizenga J., Bom V. R., Hollander R. W. and Van Eijk C. W. E., *IEEE Trans. Nucl. Sci.*, **45** (1998) 576.
[13] Fiorini C., Longoni A., Perotti F., Labanti C., Lechner P. and Strüder L., *Nucl. Instrum. Methods Phys. Res. A*, **409** (1998) 395.
[14] Nassalski A., Kapusta M., Batsch T., Wolski D., Mockel D., Enghardt W. and Moszynski M., *Nuclear Science Symposium Conference Record, 2005 IEEE, 23-29 Oct. 2005*, Vol. **5**, pp. 2823-2829.
[15] Fiorini C., Gola A., Zanchi M., Longoni A., Soltau H. and Strüder L., *Nucl. Instrum. Methods Phys. Res. A*, **571** (2007) 126.
[16] Kapusta M., Moszynski M., Balcerzyk M., Lesniewski K. and Szawlowski M., *IEEE Trans. Nucl. Sci.*, **47** (2000) 2029.
[17] Quarati F., Bos A. J. J., Brandenburg S., Dathy C., Dorenbos P., Kraft S., Ostendorf R. W., Ouspenski V. and Alan Owens F., *Nucl. Instrum. Methods Phys. Res. A*, **574** (2007) 115.